ADVANCED HEALTHCARE MATERIALS
www.advhealthmat.de

Elevating Platinum to Volumetric Capacitance: High Surface Area Electrodes through Reactive Pt Sputtering

*Maciej Gryszel, Marie Jakešová, Xuan Thang Vu, Sven Ingebrandt, and Eric Daniel Głowacki**

Platinum is the most widespread electrode material used for implantable biomedical and neuroelectronic devices, motivating exploring ways to improve its performance and understand its fundamental properties. Using reactive magnetron sputtering, PtO_x is prepared, which upon partial reduction yields a porous thin-film form of platinum with favorable properties, notably record-low impedance values outcompeting other reports for platinum-based electrodes. It is established that its high electrochemical capacitance scales with thickness, in the way of volumetric capacitor materials like IrO_x and poly(3,4-ethylenedioxythiophene), PEDOT. Unlike these two well-known analogs, however, it is found that PtO_x capacitance is not caused by reversible pseudofaradaic reactions but rather due to high surface area. In contrast to IrO_x, PtO_x is not a reversible valence-change oxide, but rather a porous form of platinum. The findings show that this oxygen-containing form of Pt can place Pt electrodes on a level competitive with IrO_x and PEDOT. Due to its relatively low cost and ease of preparation, PtO_x can be a good choice for microfabricated bioelectronic devices.

1. Introduction

Platinum is the most common biointerface electrode material for neurostimulation and neural recording electrodes. Presently, nearly all chronically implanted bioelectronic medicine devices, such as deep brain stimulators, peripheral nerve interfaces, implanted encephalography electrodes, and spinal cord stimulators utilize platinum as the active electrode.[1–3] Platinum is regarded as a noble metal with suitable biocompatibility. Its double-layer capacitance and charge storage/injection capacity are, however, relatively low compared to many next-generation neural interface electrode materials such as TiN, conducting polymers, and IrO_x.[4,5] To boost the interfacial capacitance of Pt to more competitive levels, various techniques for micro- and nano-structuring of platinum have been explored. Platinum electrodes can be roughened and porosified by laser ablation,[6] or by electrochemical treatments.[7] These procedures enhance the exposed surface area of the platinum, increasing capacitance and leading to a drop in electrochemical impedance. The most-explored method for preparation of high surface-area ultra-low-impedance platinum is electrochemical deposition of structured platinum from platinum salt solutions.[8,9] These porous structures are sometimes referred to as platinum black or grey, and can feature various shapes of nano or microstructured Pt. Prominent examples include *Pt nanograss*[9] or *nanoPt*[10] coatings reported by Asplund and coworkers, demonstrated for in vitro and in vivo applications.[10] These coatings represent the to-date best reports in terms of low impedance platinum (e.g., |Z| @ 1 kHz between 20–50 kΩ for 35 µm diameter electrodes). Nevertheless, the key performance metrics of platinum electrodes lag behind the aforementioned emerging neural interface materials.

Herein we take an alternative approach to improving the electrochemical properties of Pt: preparation of partially bulk-oxidized PtO_x films by reactive magnetron sputtering. This builds upon our recently published method of preparation of porous noble metal films by (electro)chemical reduction of sputtered noble metal oxides (Au, Pd, and Pt).[11] In this earlier work we found that unlike the other "noble" metals, reduction of PtO_x proceeded only partially and a high level of oxygen content always remained in the bulk of the films regardless of treatment conditions. Inspired by this finding, herein we have set out to characterize sputtered PtO_x as an electrode material in the context of bioelectronics applications. To this end, we prepare electrodes based on reactively sputtered PtO_x (**Figure 1**A,B) and compare them with

M. Gryszel
Laboratory of Organic Electronics
Department of Science and Technology
Linköping University
Bredgatan 33, Norrköping 60174, Sweden
M. Jakešová, E. D. Głowacki
Bioelectronics Materials and Devices Laboratory
Central European Institute of Technology
Brno University of Technology
Purkyňova 123, Brno 61200, Czech Republic
E-mail: eric.daniel.glowacki@ceitec.vutbr.cz
X. T. Vu, S. Ingebrandt
Institute of Materials in Electrical Engineering 1
RWTH Aachen University
52074 Aachen, Germany

The ORCID identification number(s) for the author(s) of this article can be found under https://doi.org/10.1002/adhm.202302400

DOI: 10.1002/adhm.202302400

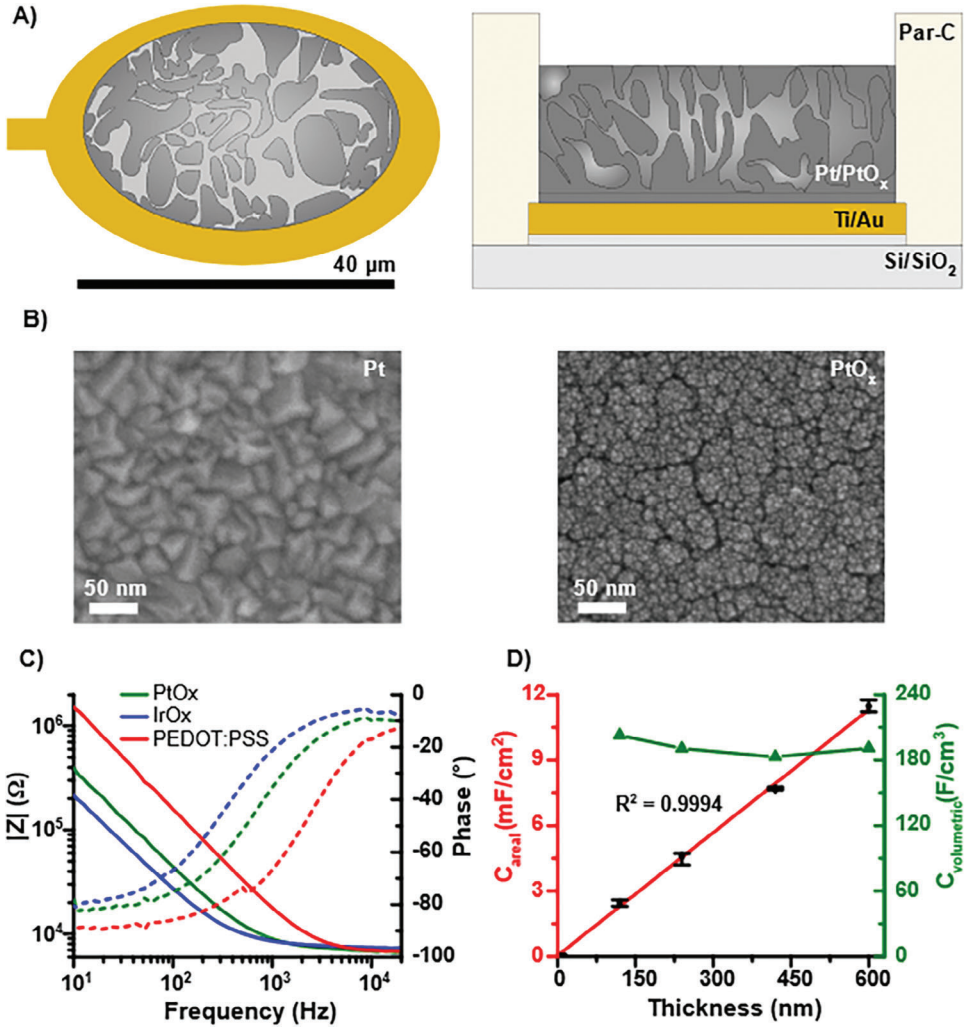

Figure 1. A) Cross section schematic of microelectrodes tested in this study: Ø 40 µm Au microelectrodes coated with PtO_x. B) Scanning electron microscopy (SEM) micrographs of a planar Pt film, versus a PtO_x film. The PtO_x shows a fine microporous structure. C) Electrochemical impedance spectra (solid line – modulus, dashed line – phase angle) of Ø 40 µm Au microelectrodes coated with 240 nm of PtO_x, PEDOT:PSS (crosslinked with GOPS), or IrO_x (after electrochemical activation described in the experimental section). Impedance of planar Pt electrodes of the same size (not shown), give |Z| (≈450 kΩ @ 1 kHz). D) Areal and volumetric capacitance of PtO_x (135 W DC sputtering at 47 mTorr of Ar with 20% O_2) layers of different thickness, deposited on Ø 40 µm Au microelectrodes. Calculations were done based on cyclic voltammetry data. Areal capacitance linearly scales up with PtO_x thickness up to 600 nm, thicker samples have only slightly increased areal capacitance and lower volumetric capacitance. Increasing thickness beyond this point leads to an increase in series resistance, which may originate from the poor conductivity of the PtO_x bulk film,[12] and/or so-called pore resistance, and small electrolyte-filled channels introduce electrochemical impedance.

two well-known high-capacity/low-impedance electrodes used in bioelectronics: poly(3,4-ethylenedioxythiophene):poly(styrene sulfonate), PEDOT:PSS, and IrO_x. These materials serve as points of reference to help understand both the performance and electrochemical nature of PtO_x electrodes.

2. Results and Discussion

2.1. Capacitive Properties of PtO_x

We characterized the electrochemical impedance of Ø 40 µm PtO_x microelectrodes, and estimated the electrochemical capacitance of PtO_x films using cyclic voltammetry (details on film preparation can be found in Section 2.2). The impedance of these is significantly lower than planar Pt, and lower than previous reports on best-of structured Pt microelectrodes (we achieve ≈8.6 kΩ @ 1 kHz, compared with values >20 kΩ reported in the literature for the same sized electrodes, Ø 35–40 µm).[13] In a side-by-side comparison, our measured impedance is on-par with pseudofaradaic coatings PEDOT:PSS and IrO_x (Figure 1C). Moreover, the most remarkable result was that the two-dimensional areal capacitance of PtO_x was not only relatively high (Figure 1D), but the measured capacitance scaled linearly with the thickness of the deposited PtO_x layer, in the same manner as the so-called volumetric capacitor materials PEDOT and IrO_x. We calculate a volumetric capacitance of 200 mF cm^{-3}, a value on-par with the best optimized PEDOT formulations.[14] This finding begs the question as to the mechanism behind this high capacity. PE-

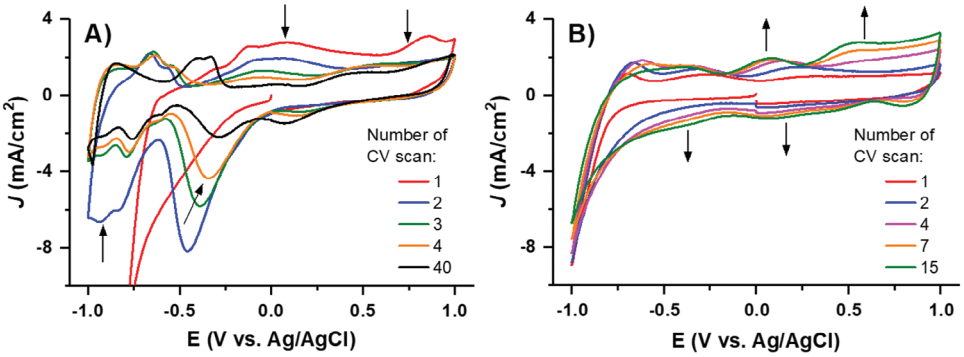

Figure 2. Cyclic voltammetry scans (100 mV s^{-1}, deoxygenated PBS of pH 7.4) registered in −1.0 to +1.0 V versus Ag/AgCl range for fresh samples of: A) PtO_x, B) IrO_x. While the IrO_x sample shows a progressive increase in electrochemical capacitance, known as electrode "activation," PtO_x shows the opposite behavior where the features of the CV evolve to resemble those of Pt. By 40 scans, the scan stabilizes, and PtO_x films behave essentially as Pt of a high surface area. Film thickness = 240 nm, area of the samples = 0.05 cm^2. Impedance of PtO_x and volumetric capacitance remain unchanged via this procedure.

DOT and IrO_x store charge in their volume due to pseudofaradaic reactions.[4] The PEDOT chains can be reversibly oxidized and reduced, and counter ions can be transported in and out of the PEDOT layer.[15] In IrO_x, reversible redox reactions are available, especially the Ir^{3+}/Ir^{4+} couple. This makes IrO_x a valence-change oxide which can reversibly store charge in its bulk. We performed a series of experiments to test if the bulk of the PtO_x behaves analogously to IrO_x, with bulk electrochemical reversibility. It is well-established that the surface of platinum is reversibly oxidized, as an oxide forms during anodic polarization and is subsequently reduced during a cathodic scan.[16] The question is if platinum oxide in the bulk is electrochemically accessible to redox activity in a way analogous to IrO_x. Our experiments show that in a potential window relevant for bioelectronics, i.e., neurostimulation, there is no evidence for bulk reversibility. In repeated cyclic voltammetry scans from +1 to −1 V versus Ag/AgCl in deoxygenated PBS (**Figure 2**) we see a decrease in peak amplitude and area on PtO_x, to yield a CV reminiscent of normal Pt, albeit with high capacitance (Figure 2A). The first few scans show high reduction currents, which we interpret as electrochemically accessible platinum oxides being reduced to platinum. Over the course of 40 cycles, the CV stabilizes to a familiar one for Pt. Even the highly characteristic proton adsorption peaks[16] from the formation of Pt-H are apparent. This reversion of the CV characteristics to those resembling platinum would indicate that the PtO_x sample is, net, electrochemically behaving as Pt itself, and the oxide is buried within electrochemically inaccessible fractions of the sample. IrO_x electrodes, under the same scanning conditions, show progressively higher amplitude peaks, both cathodic and anodic, over the whole scan range (Figure 2B).[4] This process of increasing charge storage capacity is indicative of increasing hydration of the layer and high reversibility of the Ir redox reactions, and is in the literature on such electrodes known as activation or preconditioning. The exchange of H^+ and OH^- into the layer is reported to accompany the valence change reactions of Ir.[17] Thus, well-hydrated IrO_x layers are associated with high electrochemical capacitance. This analogous "activation" process does not appear in PtO_x films. We can surmise that these PtO_x layers consists of porous conductive support, which from energy-dispersive X-ray spectroscopy (EDX) we can conclude is largely oxidized, with electrochemically active platinum at the surface.

The irreversibility of PtO_x redox behavior is corroborated by measuring oxygen content in the films before and after galvanostatic reduction and then reoxidation. If the reaction were reversible, reduction is expected to yield lower measured oxygen content while reoxidation should restore the oxygen content. While there is a small degree of reversibility of oxygen content apparent in PtO_x during reduction/reoxidation due to well-known surface oxidation/reduction, the level of reversibility is much higher in IrO_x samples (**Table 1**). This distinction in reversibility we found is also apparent in experiments of repeated CVs (2600 cycles in −0.3 to +0.1 V vs Ag/AgCl range). While the oxygen content of PtO_x falls, IrO_x retains its original stoichiometry (Table 1). The oxygen stoichiometry imbalance can be mechanistically rationalized in the following way: The galvanostatic application of negative current can drive faradaic reactions like water reduction, while galvanostatic application of positive current leads to oxidation of exposed metallic platinum, but only at the electrochemically accessible surface. Most of the current goes into water oxidation. It is well-established that water oxidation proceeds electrocatalytically from the oxidized platinum surface.[18] The formation of a surface oxide is well-established, but the oxide thickness is very limited and does not ingress into the film with higher applied voltage. Meanwhile, in IrO_x, electrochemical redox reactions occur throughout the bulk of the sample, allowing the oxygen content to change.

To further probe the distinction in electrochemical reactions occurring at PtO_x versus IrO_x, we measured electrochemical capacitance in aqueous and nonaqueous electrolyte using 0.05 M $LiClO_4$, as this electrolyte salt is soluble in both water and acetonitrile. The results are shown in **Table 2**. In the case of IrO_x, the measured capacitance decreases by a factor of three when measured in nonaqueous electrolyte. This can be understood since without water, the pseudofaradaic reactions affording the high capacity are blocked. These reactions require exchange of H^+ and H_2O with the bulk of the film. We do not observe this kind of drop in capacitance for PtO_x, however. In fact, the measured capacitance value is about 10% higher in acetonitrile than in water. This signals that the charge storage mechanism in PtO_x does

Table 1. Change in the oxygen content in layers (100 nm) subjected to electrochemical reduction and reoxidation treatments. Due to limitations of the EDX assay,[11] the results should be treated as semi-quantitative.

Electrochemical experiment	Stage of the experiment	O content [atom%] by EDX	
		PtO_x	IrO_x
Galvanostatic reduction/reoxidation: *high current density*	Fresh sample	45.2	47.3
	After reduction: −5 mA cm^{-2}, 60 s	22.9	40.9
	After reoxidation: +5 mA cm^{-2}, 60 s	26.3	46.0
	Recovery of initial O content (atom%)	15.0%	80.0%
Galvanostatic reduction/reoxidation: *low current density*	Fresh sample	45.2	48.1
	After reduction: −70 µA cm^{-2}, 2500 s (3.5 mC)	37.4	41.5
	After reoxidation: +40 µA cm^{-2}, 4750 s (3.8 mC)	39.6	47.3
	Recovery of initial O content (atom%)	27.1%	87.5%
CV cycling: −0.3 to +0.1 V, 100 mV s^{-1}	Fresh sample	45.2	47.6
	After 2600 CV cycles (5 h 45 ′)	37.6	47.4
	Decrease of the O content (atom%)	17.5%	0.4%

not require aqueous ion exchange as in IrO_x. The higher measured capacitance for nonaqueous conditions in PtO_x can be explained by the lower viscosity of acetonitrile, which allows better electrolyte penetration into the porous structure of PtO_x. Taken together, these results all implicate the PtO_x film as a porous double-layer capacitance Pt material with faradaic properties resembling Pt, and not the pseudofaradaic mechanism postulated for the valence-change oxide IrO_x.

2.2. Optimizing Deposition Conditions for PtO_x Electrodes

We tuned the reactive sputtering conditions (sputtering pressure, power, DC versus RF plasma, and oxygen:argon ratio) to yield an optimized PtO_x with respect to high electrochemical capacity and low impedance. We also estimated the oxygen content in the films. Varying the sputtering conditions, when considering the final oxygen content of the film as estimated by EDX analysis, several trends are apparent: First, more oxygen added in the sputtering mixture always correlates with higher oxygen content. For a fixed Ar:O_2 ratio, DC sputtering always yields less oxygen content than the analogous process using RF. Regardless of plasma type, increasing power always correlates with less oxygen content. Overall working pressure does increase oxygen content, also the working pressure has a substantial effect on film roughness and morphology. While these different parameters may yield porous PtO_x films suitable for many interesting applications, ranging from catalysis to biosensors, our present focus is on low-impedance/high capacity electrodes for bioelectronics. Therefore, we evaluated those two parameters only, and in a direct comparison (**Table 3**) the best-performing films are prepared via the following conditions: (DC, 135 W, 47 mTorr, 20% O_2). This optimized coating of PtO_x was compared in microelectrodes with two well-known low impedance coatings: PEDOT:PSS and IrO_x. This yielded the comparison of impedance shown in Figure 1C.

Table 2. Capacitance values calculated from CV scans in aqueous versus nonaqueous electrolytes. Film thickness = 100 nm.

Material	Electrolyte solvent	Areal capacitance [mF cm^{-2}]
IrO_x	Acetonitrile	0.41
	H_2O	1.17
PtO_x	Acetonitrile	1.17
	H_2O	1.06

2.3. Biofouling Tests and Comparative Stability

During operation of bioelectronics devices, physiological conditions represent a harsh environment and the issue of biofouling is important. Adhesion of proteins and other biomolecules on the surface can severely degrade performance of electrode materials. We compared samples made using the optimized protocol (DC 135 W, 47 mTorr, 20% O_2) with IrO_x and PEDOT as references. In these experiments, we prepared MEAs with Ø 40 µm micro-

Table 3. Estimated oxygen content in PtO_x layers (120 nm) and electrochemical capacity as a function of different sputtering parameters. Due to safety limitations of the sputtering system, depositions are limited to <20% O_2 in the sputtering gas mixture. *Sample thickness homogeneity was low, therefore reasonable estimation of capacitance was N/A.

PtO_x preparation procedure	O content [atom%] by EDX	Capacitance [mF cm^{-2}]
Ref. [11] procedure, Electrochemical reduction −0.8 V 60 s	44.9	0.612
RF 60 W, 25 mTorr, 15% O_2	56.1	N/A*
RF 135 W, 25 mTorr, 15% O_2	50.3	1.159
RF 135 W, 30 mTorr, 15% O_2	51.3	1.220
RF, 135 W, 47 mTorr, 20% O_2	55.5	1.305
DC 135 W, 28 mTorr, 20% O_2	40.5	0.763
DC 135 W, 37 mTorr, 20% O_2	44.5	1.216
DC, 60 W, 47 mTorr, 20% O_2	50.6	N/A*
DC 135 W, 47 mTorr, 20% O_2	45.2	1.517

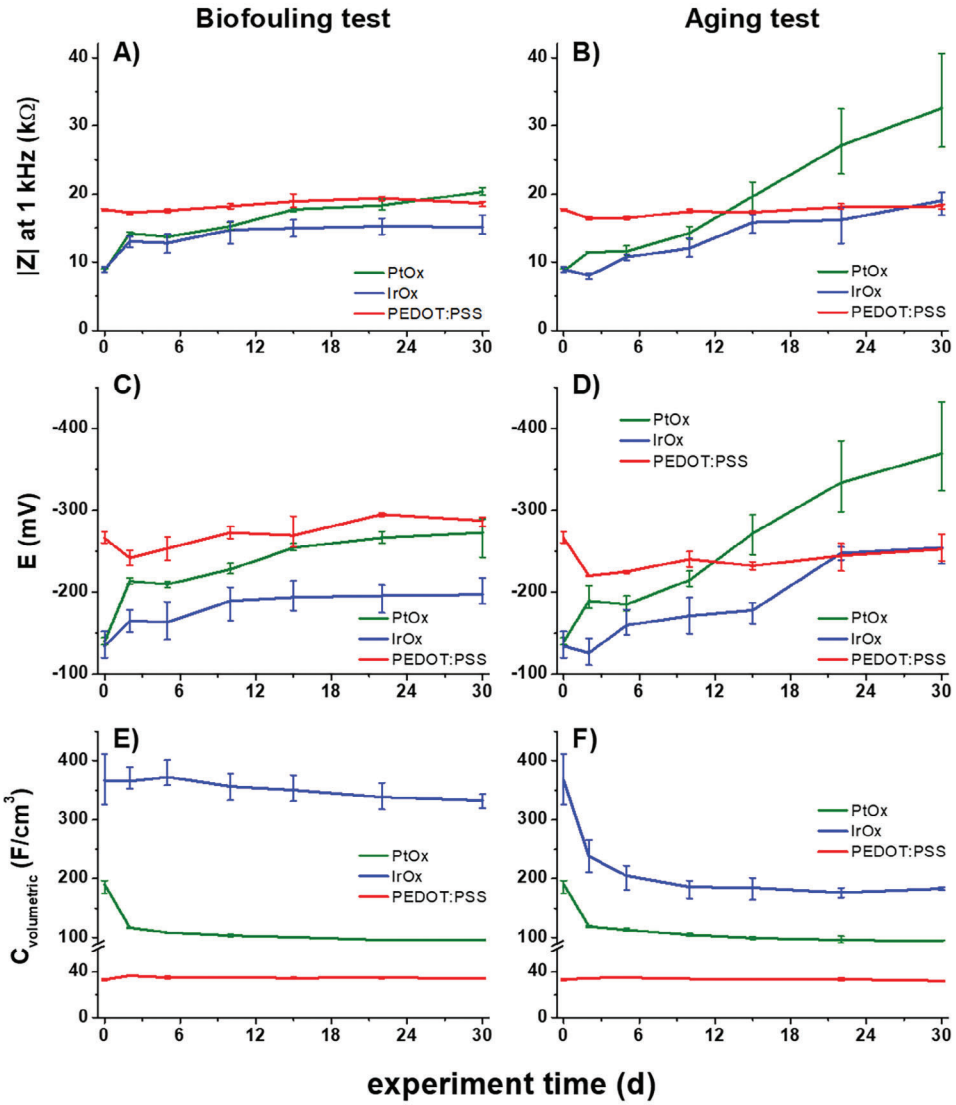

Figure 3. Relative stability of PtO_x, IrO_x, and PEDOT:PSS layers (240 nm, on Ø40 µm Au microelectrodes) subjected to biofouling (A, C, and E) and accelerated aging tests at 60° (B, D, and F). A,B) Change in absolute impedance at 1 kHz. C,D) Change in peak voltage values of cathodic phase of 200 µC cm^{-2} phase^{-1} biphasic pulse. These are cathodic voltage excursions from baseline measured versus an AgCl reference electrode in three-electrode configuration. E,F) Change in volumetric capacitance. All results for given material are averaged over 3–4 different microelectrodes. Samples are removed from the aging chamber and measured, then returned to the given aging condition.

electrodes made of planar gold, coated with 240 nm of each of the respective coatings.

The stability of the MEA samples was evaluated in two sets of stability tests: The first addressed longer-term biofouling, where the samples were stored in 2% bovine serum albumin in 1× PBS at 37 °C over the course of 30 days. The second was an accelerated aging test, where the samples were stored in 1× PBS at 60 °C. Over the course of both of these protocols, samples were regularly removed and tested via impedance measurements, CV cycles, and a measurement of voltage excursions during application of biphasic current stimulation pulses with 200 µC cm^{-2} phase^{-1}. The results of key figures of merit: impedance value at 1 kHz, volumetric capacitance values, and cathodic voltage excursion during pulsing show a critical comparison between the three coatings (**Figure 3**). PEDOT and IrO_x generally outperform PtO_x in terms of % change over time, though PtO_x layers demonstrated some surprising qualities such as stable volumetric capacitance which was consistently more than twice as high as that of PEDOT. Overall, the long-term stability of PtO_x, however, was poorer than the reference samples IrO_x and PEDOT. Though the performance of PtO_x decreased, impedance remains an order of magnitude better than Pt alone. We would speculate that the decline in PtO_x performance is due to aggregation effects which lead to a decrease in effective surface area to some extent.

3. Conclusions

PtO_x, prepared by reactive sputtering, represents an interesting and potentially competitive variation to the range of platinum modifications that are being pursued in the bioelectronics field.

Its preparation is fully compatible with microprocessing, easily integratable with lithography for instance. The many variables available in reactive sputtering techniques, of which we have only explored a few, can potentially provide a wider palette of functional properties to PtO_x thin films. From a fundamental point of view, we have critically addressed the question of charge storage mechanism in these films: they are essentially a highly porous variety of platinum. Macroscopically, these films show a remarkable „volumetric capacitance", with capacitance scaling with thickness. The volumetric capacitance values exceed, by more than a factor of two, the well-known material PEDOT:PSS. Through a series of electrochemical and elemental analysis we compare PtO_x with IrO_x. Using these comparative methods, we show, that the high volumetric capacitance effect in PtO_x originates from high porosity of the films rather than a bulk reversible redox chemistry as is the case of IrO_x (or PEDOT:PSS). The observation suggests that the concept of volumetric capacitance does not necessarily apply only to pseudofaradaic materials. In terms of bioelectronic microelectrodes, the PtO_x brings platinum to the level of competitive parameters for impedance and capacitance to the next-generation materials like IrO_x and PEDOT. In contrast to IrO_x, PtO_x works well already "as-fabricated" and does not require extensive electrochemical conditioning. By virtue of ease of processability and especially much lower cost compared to IrO_x, the use of PtO_x may be indicated in many applications for microfabricated bioelectronics devices.

4. Experimental Section

Materials: Sputtering targets for Vaksis 3 м system (2.00″ Dia. × 0.125″ thick) were supplied by Testbourne Ltd (Pt, 99.99%) and Nordic High Vacuum AB (Au, 99.99%). PEDOT:PSS (Clevios PH1000 formulation) was supplied by Hereaus. Dichloro[2.2]paracyclophane (Parylene-C precursor) was supplied by TiXX Coatings Ltd. All other chemicals were supplied by Sigma-Aldrich and used without any purification. Bovine albumin serum used in the stability tests was the heat shock fraction, pH 5.2, ≥96%.

Preparation of Au Coated Substrates for Electrodes of 0.05 cm² Active Area: PET foil (Policrom screens, 120 µm thick) was selected as a substrate due to the fact that it provides good adhesion for layers of sputtered Au without the need of any additional sticking layer. Before Au deposition, the foil was cut to rings of Ø 11.5 cm and cleaned by subsequent sonication (10 min) in isopropanol and DI water. After drying, it was loaded into a Vaksis 3 м sputtering system without any pre-activation with oxygen plasma or ozone. After evacuation of the vacuum chamber to pressure $<1 \times 10^{-5}$ Torr, Au layer (100 nm) was sputtered at 3.8–4.0 mTorr pressure of pure argon using a DC magnetron at 100 W.

Reactive Sputtering of PtO_x: All depositions of metal oxides were done by magnetron sputtering using an $Ar:O_2$ mixture. The pressure was regulated with the gate valve and rotation velocity of the turbomolecular pump. The substrates were never heated. To fabricate 0.05 cm² electrodes, Au-coated PET foil was cut with scissors to pieces of ap. 2 × 2 cm size (appropriate for the cell used for the electrochemical characterization) which were mounted by the edges to the sample holder with Kapton tape. After PtO_x deposition, active area of the layer was limited to 0.05 cm² with a self-adhesive foil (with Ø 2.5 mm opening). In the case of microelectrodes, before loading to the sputtering chamber, substrates were treated with oxygen plasma (50 W, 120 s, Diener electronic GmbH). Deposition of the PtO_x was preceded (in the same vacuum cycle) by sputtering of a smooth layer of Pt (10 nm) to improve adhesion of the oxide coating. In the case of MEA samples in the final step of the fabrication sacrificial Parylene-C layer was peeled off with the assistance of Kapton tape, air stream and if needed, mild sonication in DI water.

Thickness Control of the Sputtering Deposited Layers in Vaksis 3 м System: Thickness of all layers was controlled by the duration of the process (based on the known and well-reproducible values of rate) and always in good accordance with readings of quartz crystal monitor of the sputtering system. Tooling factors, as well as the values of rate, were predetermined by time-controlled sputtering on glass substrates, with thickness measured with a Dektak XT (Bruker) profilometer.

Fabrication of Microelectrode Samples: Silicon wafers with 2.5 µm thermally grown oxide layer were used as the substrate. The metal leads and interconnects consisting of 20 nm Ti and 50 nm Au were deposited by an electron-beam evaporation system (BESTEC), patterned by photolithography (AZ 1518) and etched with $KI:I_2:H_2O$ gold etchant and $HF:H_2O_2:H_2O$ titanium etchant. The encapsulation was provided with a 2 µm layer of Parylene-C (SCS Labcoter) grown by chemical vapor deposition in presence of an adhesion promoting silane A-174. The metal pads were exposed by photolithography (AZ 1518) and reactive ion etching (RIE, O_2 plasma, 200 W). To facilitate the patterning of the electrode coating materials (IrO_x, PtO_x, and PEDOT:PSS), another, sacrificial, layer of 2 µm Parylene-C was deposited on top of the encapsulation layer with a 2% Micro-90 anti-adhesive coating in between. The electrode area (40 µm diameter) was exposed by photolithography (AZ 9260) and reactive ion etching (RIE, O_2 plasma, 200 W). Thus prepared substrates were activated by an O_2 plasma just before deposition of the electrode material. The sacrificial Parylene-C layer was then peeled off to yield the microelectrode array.

PEDOT:PSS was deposited by spin coating from a sonicated dispersion of PEDOT:PSS (Clevios PH 1000, Heraeus), 5 wt% ethylene glycol, 0.1 wt% dodecyl benzene sulfonic acid, and 1 wt% of (3-glycidyloxypropyl)-trimethoxysilane (added and mixed just before the spin coating). After the peel-off, the PEDOT:PSS layer was annealed at 140 °C for 45 min.

IrO_x was deposited by magnetron sputtering according to previously published methods,[17] and patterned via Parylene-C peel-off as described above.

SEM Imaging and EDX Analysis: SEM imaging and EDX analysis were performed with SEM Zeiss Sigma-500, equipped with Bruker Nano XFlash 610 м Detector (silicon drift detector (SDD), with thermoelectric (Peltier) cooling and light element window), set at elevation angle 35°. All samples were contacted to the microscope stage using copper tape, after washing with DI water and drying in a stream of N_2. Images were taken with the in-lens secondary electron detector at an acceleration voltage of 7–15 kV, 30 µm beam aperture, and 3.3–3.6 mm working distance, with the chamber evacuated to pressure $<1 \times 10^{-5}$ mbar. Electron beam shift was used to move the imaging area without introducing vibrations.

In EDX analysis, the P/B-ZAF standardless method was always used with carbon deconvolution, fast quantification correction, and following spectral lines: 0.525 keV for O (Kα) and 2.048 keV for Pt (M). To maximize the detector count rate, the working distance was 10–11 mm, the beam aperture was set to 120 µm with the high current mode enabled. To compensate for surface roughness and possible sensitivity of the noble metal oxides to the electron beam, low image magnification (×1000) and acceleration voltage (6 kV) were always used. Results, given as Pt/O atom%, were averaged over 6 measurements, done in different parts of the specimen. Variability (as relative standard deviation) was relatively low (lower than the relative assay error, calculated by the software). Using higher acceleration voltages (up to 12 kV) usually gave similar values of atom% but with higher variability. For the purpose of the analysis, in order not to overestimate metal content in the oxide, to eliminate signal coming from the substrate a designated set of samples was prepared, in an analogous way like for the electrochemical characterization without 10 nm of smooth Pt interlayer.

Electrochemical Characterization: Characterization of all samples was done with an Ivium technologies *Vertex One* potentiostat and phosphate buffer saline (1× PBS: 10 mM phosphate, pH 7.4; 138 mM NaCl, 2.7 mM KCl in DI water) as the electrolyte. 0.05 cm² samples were electrically contacted with copper tape (attached to the uncoated area of the substrate) and placed in a 15 mL double-sided electrochemical cell (Redox.me), equipped with a Pt coil as a counter electrode, and an Ag/AgCl wire as a pseudoreference electrode. The electrolyte was deoxygenated before measurements by purging with argon. Microelectrodes were measured with

platinum plate as counter electrode and Ag/AgCl pseudoreference electrode confined in a syringe, filled with the electrolyte by adjusting the pressure with another syringe connected by a flexible tubing. The sample was precisely positioned under the syringe tip to achieve the electrolytic contact without any mechanical connection. The electrical contact was carefully established with a needle probe placed on the contact pad. In case of microelectrode measurements, deoxygenation of the electrolyte was not possible. The cyclic voltammetry experiments were performed with the 100 mV s^{-1} scan rate and +0.1 to +0.3 V scanning range for the purpose of estimating capacitance of the electrodes. Scans are conducted in this range to obtain a stable capacitive-charging type transient current, this behavior stabilizes after the first scan. Electrochemical double-layer capacitance was calculated by integrating the current in this charging/discharge region, according to the equation described in Chapter 1 of the Bard and Faulkner textbook.[19] Electrochemical impedance spectra were recorded using a single-sine probing AC voltage of 10 mV amplitude at a DC bias of 0 V versus the reference electrode with 20 points per decade. Biphasic pulsing stress test was done using the same equipment to a charge density of 200 µC cm^{-2} $phase^{-1}$ in the following sequence: 50 µs rest time (with $I = 0$ A), 250 µs cathodic-leading square waveform, 50 µs interpulse time ($I = 0$ A), 250 µs anodic square waveform, 50 ms rest time (with $I = 0$ A). The result (as $V = f(t)$ curve, measured vs Ag/AgCl pseudoreference electrode with 10 µs interval time) was averaged over 10 consecutive pulses. The peak value of the cathodic phase is given as voltage versus baseline (averaged V recorded during initial 50 µs of the pulsing sequence).

Acknowledgements

The authors thank Mary Donahue for help with PEDOT sample preparation. This work has been supported by the European Research Council (ERC) under the European Union's Horizon 2020 research and innovation program (E.D.G. grant agreement No. 949191), by the Grant Agency of the Czech Republic under contract 23-07432S, and by funding from the National Center for Neurological Research, supported by the MEYS CR (LX22NPO5107). Sample fabrication was supported by CzechNanoLab Research Infrastructure supported by MEYS CR (LM2023051).

Open access publishing facilitated by Vysoke uceni technicke v Brne, as part of the Wiley - CzechELib agreement.

Conflict of Interest

The authors declare no conflict of interest.

Data Availability Statement

The data that support the findings of this study are available from the corresponding author upon reasonable request.

Keywords

bioelectronics, biomedical microdevices, electrochemistry, platinum, reactive sputtering

Received: July 26, 2023
Revised: May 14, 2024
Published online:

[1] E. S. Krames, P. H. Peckham, *Neuromodulation*, (Eds.: A. R. Rezai), Academic Press, London **2009**.
[2] D. R. Merrill, in *Implantable Neural Prostheses 2* (Eds.: D.D. Zhou, E. Greenbaum), Springer Science+Business Media, New York, NY **2010**, pp. 85–138.
[3] I. Gablech, E. D. Głowacki, *Adv. Electron. Mater.* **2023**, *9*, 2300258.
[4] S. F. Cogan, *Annu. Rev. Biomed. Eng.* **2008**, *10*, 275.
[5] P. Fattahi, G. Yang, G. Kim, M. R. Abidian, *Adv. Mater.* **2014**, *26*, 1846.
[6] R. A. Green, P. B. Matteucci, C. W. D. Dodds, J. Palmer, W. F. Dueck, R. T. Hassarati, P. J. Byrnes-Preston, N. H. Lovell, G. J. Suaning, *J. Neural Eng.* **2014**, *11*, 056017.
[7] A. N. Ivanovskaya, A. M. Belle, A. M. Yorita, F. Qian, S. Chen, A. Tooker, R. G. Lozada, D. Dahlquist, V. Tolosa, *J. Electrochem. Soc.* **2018**, *165*, G3125.
[8] S. A. Desai, J. D. Rolston, L. Guo, S. M. Potter, *Front. Neuroeng.* **2010**, *3*, 5.
[9] C. Boehler, T. Stieglitz, M. Asplund, *Biomaterials* **2015**, *67*, 346.
[10] C. Boehler, D. M. Vieira, U. Egert, M. Asplund, *ACS Appl. Mater. Interfaces* **2020**, *12*, 14855.
[11] M. Gryszel, M. Jakešová, T. Lednický, E. D. Głowacki, *Adv. Mater. Interfaces* **2022**, *2022*, 2101973.
[12] H. Neff, S. Henkel, E. Hartmannsgruber, E. Steinbeiss, W. Michalke, K. Steenbeck, H. G. Schmidt, *J. Appl. Phys.* **1996**, *79*, 7672.
[13] C. Boehler, S. Carli, L. Fadiga, T. Stieglitz, M. Asplund, *Nat. Protoc.* **2020**, *15*, 3557.
[14] S. Kim, C. Kim, Y. Kim, N. Kim, W. Lee, E. Lee, D. Kim, S. Park, K. Lee, J. Rivnay, M. Yoon, *Nat. Commun.* **2018**, *9*, 3858.
[15] B. D. Paulsen, K. Tybrandt, E. Stavrinidou, J. Rivnay, *Nat. Mater.* **2020**, *19*, 13.
[16] A. Weltin, J. Kieninger, *J. Neural Eng.* **2021**, *18*, 052001.
[17] A. Van Ooyen, G. Topalov, G. Ganske, W. Mokwa, U. Schnakenberg, *J. Micromech. Microeng.* **2009**, *19*, 074009.
[18] V. I. Birss, A. Damjanovic, P. G. Hudson, *J. Electrochem. Soc.* **1986**, *133*, 1621.
[19] A. J. Bard, L. R. Faulkner, *Electrochemical Methods Fundamentals and Applications*, John Wiley & Sons, New York **2001**.